Macromolecules

pubs.acs.org/Macromolecules Article

Cyclic Topologies in Linear α,ω-Dihydroxy Polyisoprenes by Dielectric Spectroscopy

Achilleas Pipertzis, Konstantinos Ntetsikas, Nikos Hadjichristidis,* and George Floudas*

Cite This: *Macromolecules* 2022, 55, 10491−10501 Read Online

ACCESS | Metrics & More | Article Recommendations | Supporting Information

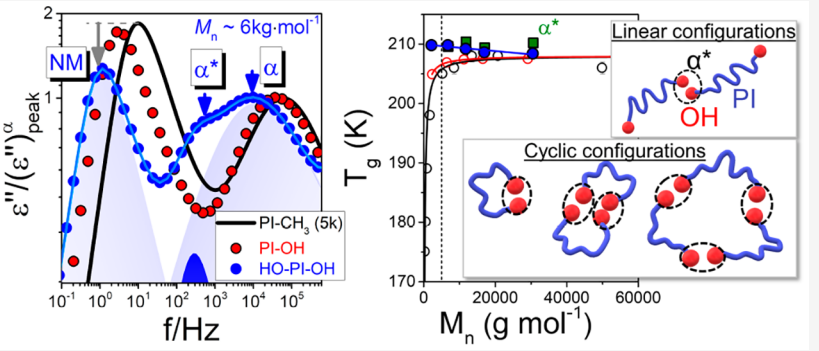

ABSTRACT: A series of mono- and di-functionalized polyisoprenes (PIs) bearing hydroxyl (OH−) end-group(s) with different molar masses ranging from 2 to 30 kg mol^{-1} were synthesized and studied by a combination of temperature- and pressure-dependent dielectric spectroscopy and rheology. In the di-functionalized PIs, the −OH end-group interactions result in a mixture of linear and cyclic configurations (up to 45% cyclic configurations for the lower molar masses). The formation of cyclic topologies due to increased H-bonding interactions restricted the backbone mobility and increased the glass temperature, T_g, especially for the lower molar masses. Moreover, an additional process (termed α^*) was evidenced in the dielectric spectroscopy in the range between the segmental process and the global chain relaxation. It followed a Vogel−Fulcher−Tammann temperature dependence, freezing at a temperature in the vicinity of the liquid-to-glass temperature, being independent of molar mass. Its molecular origin was identified by employing the pressure sensitivity of the characteristic relaxation times and the pressure dependence of T_g. It reflects the relaxation of segments in the vicinity of the H-bonded groups. Overall, this study provided information on the impact of weakly associating polar end-groups (hydroxyl) on the molecular dynamics of type-A polymers. Furthermore, it suggested promising routes for designing polymers with a higher concentration (>50%) of cyclic topologies, for example, by employing (i) short chains with (ii) strongly associating end groups (stronger than the hydroxyl end-groups).

1. INTRODUCTION

Telechelic polymers are promising materials for biomedical applications (e.g., bioconjugates and hybrid nanostructures) as well as for advanced technological areas (e.g., self-healing materials, thermoplastic elastomers, pressure-sensitive adhesives, colloidal dispersants, compatibilizers for polymer blends, foams, photovoltaics, sensors, and memory devices).[1−10] For this reason, there has been considerable progress in synthesizing functional polymers with well-defined numbers and positions of polar groups.[5] End-functionalized/telechelic polymers can bring about different self-organizing supramolecular structures and configurations due to the presence of different molecular interactions (van der Waals, Coulombic, H-bonding, $\pi-\pi$ stacking, etc.).[1−5] Specifically, hydrogen bonding (h.b.) is the most common secondary (or noncovalent) interaction in functionalized polymers due to its intrinsic directionality and variability of cohesive strength. The formation of h.b. can be fine-tuned by modifying their number, their location on the polymer backbone, and their specific chemistry (e.g., nature of donor and acceptor).

From a more fundamental point of view, the incorporation of polar groups alters the dipole moment, thus modifying/tuning the polymer dynamics. An extremely sensitive experimental probe to dipole fluctuations is dielectric spectroscopy (DS). Moreover, the best candidates in this endeavor are type-A polymers because of the presence of two components of dipole moment: one perpendicular and another along the chain contour. The perpendicular component is sensitive to fast local motions (segmental mode, SM), whereas

Received: July 23, 2022
Revised: October 21, 2022
Published: November 18, 2022

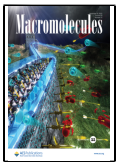

https://doi.org/10.1021/acs.macromol.2c01527
Macromolecules 2022, 55, 10491−10501

the parallel component (normal mode, NM) provides information on the fluctuations of the end-to-end vector of the chain.[11−21] Specifically, the NM is a summation of internal Rouse modes that are related to the dipole moment along the chain contour. In addition, between the Rouse modes and the segmental relaxation, the sub-Rouse process/modes can also be detected.[22,23] The times and the associated length scales of the sub-Rouse process are longer than the segment length but smaller than an entanglement strand.[22,23] The relaxation dynamics of type-A methyl-terminated PIs have been well documented in the previous studies as a function of molar mass,[11−18] temperature,[11−18] and pressure.[19−21]

The dynamics of self-associating functionalized polymers has been investigated both theoretically[24−28] and experimentally.[29−40] Specifically, the structural and rheological properties, as well as the molecular dynamics were studied, respectively, with small-angle X-ray scattering, rheology, and DS in end-functionalized type-A polymers (polyisoprene (PI) and polypropylene glycol),[29−36] and in functionalized poly(isobutylene),[37−40] polystyrene[41] (PS), polydimethylsiloxane,[42,43] and in diblock copolymers of P(S-*b*-I).[45] It was found that the polar end group interactions strongly affect the molecular dynamics.[29−40] In addition, new dielectrically active processes exist in functionalized polymers.[42−44] When the P(S-*b*-I) diblock copolymers were functionalized with zwitterionic groups (Zw-IS), a new process intermediate to the global chain and the segmental relaxation was found. It was ascribed to the segmental relaxation of regions with reduced mobility located around the polar aggregates.[44]

Herein, we report on the molecular dynamics and the chain configurations in a series of end-functionalized PIs with different (i) number of −OH end groups per chain and (ii) different chain lengths (molar masses), by employing a combination of temperature (T)- and pressure (P)-dependent dielectric spectroscopy (DS) and rheology. An additional "segmental" process was evidenced between the usual segmental and global chain relaxation. By employing the pressure dependence of the characteristic relaxation times and the pressure dependence of T_g, it was shown that it reflects the relaxation of segments in the vicinity of h.b. regions. An important finding of this work is the formation of cyclic chain configurations, comprising about half of the chain configurations for the lower molar mass polymers. The lack of free chain ends in cyclic topologies significantly affect the backbone dynamics, increasing the liquid-to-glass temperature, T_g. Evidently, by controlling the polymer molar mass and type of end-groups (hence the strength of interactions), one can "select" specific (cyclic) topologies.

2. EXPERIMENTAL SECTION

2.1. Materials. Benzene (Sigma-Aldrich, 99%), isoprene (Sigma-Aldrich, 99%), ethylene oxide (EO, Sigma-Aldrich, 99.5%), and methanol (VWR, 99.5%) were purified using high-vacuum techniques following standard procedures.[46] *sec*-Butyllithium (1.4 M in cyclohexane, Sigma-Aldrich) and 3-(*t*-butyldimethylsiloxy)-1-propyllithium (*t*BDMSOPrLi, Gelest, 0.5 M in cyclohexane) were diluted to the appropriate concentration in purified benzene under high vacuum and stored at −20 °C in suitable glass apparatuses. Tetrahydrofuran (THF, VWR, 99.5%) was dried over sodium and benzophenone. tetra-*n*-Butylammonium fluoride (TBAF, 1 M in THF) and dichloromethane (CH_2Cl_2) were purchased from Sigma-Aldrich and used without further purification.

2.2. Synthetic Procedures. The end-functionalized PIs were synthesized via conventional anionic polymerization high-vacuum techniques.[47] In all polymerizations, benzene was used as a solvent to achieve the desired high 1,4-microstructure (90−92%) of PI. For the ω-functionalized PIs, *sec*-BuLi was used as the initiator, and the polymerization was carried out at room temperature.[47] In the case of α,ω-functionalized PIs, a protected (−OH) functionalized initiator (*t*BDMSOPrLi) was used, and the polymerization was carried out at 40 °C. Subsequently, a postpolymerization reaction was performed to remove the *t*-butyldimethylsilyl (*t*BDMS) group leading to the α,ω-functionalized PI. The molecular characteristics of the functionalized PIs are presented in Table 1. The size exclusion chromatography (SEC) traces of all synthesized samples are reported in the Supporting Information (Figure S1). The synthetic details of two representative examples (PI-OH-6 kg mol^{-1} and HO-PI-OH-6 kg mol^{-1}) are described below, and the corresponding ^{1}H NMR spectra are shown in the Supporting Information (Figure S2).

Table 1. Average Molar Mass, Dispersities, and 1,4 Content for PI-OH and HO-PI-OH

sample	M_n (g mol^{-1})[a]	M_n (g mol^{-1})[b]	$Đ$[a]	1,4 content (% wt)[b]
Mono-Functionalized PIs				
PI-OH	2400	2700	1.06	91
PI-OH	6500	6900	1.03	93
PI-OH	11300	11900	1.03	92
PI-OH	16600	17200	1.02	92
PI-OH	29200	33100	1.02	92
Di-Functionalized PIs				
HO-PI-OH	2200	2500	1.07	91
HO-PI-OH	6800	6300	1.03	91
HO-PI-OH	11800	10800	1.02	92
HO-PI-OH	17000	16200	1.03	92
HO-PI-OH	30600	34500	1.02	92

[a] M_n values and $Đ$ were determined through SEC measurements in THF at 303 K calibrated with PI standards. [b] ^{1}H NMR measurements (500 MHz) were performed in $CDCl_3$ at room temperature.

2.3. Synthesis of ω-Functionalized PI (PI-OH). Isoprene (5 g) was added to 100 mL of benzene, followed by the addition of *sec*-BuLi (0.833 mmol). After 24 h, EO (∼1 mL) was introduced to the reaction mixture, kept for 8 h, and the polymerization was terminated by addition of methanol (<1 mL) (Figure 1a). The polymerization solution was poured into a large excess of methanol, and the precipitated final polymer was dried in a vacuum oven at 40 °C (M_n = 6900 g mol^{-1}, calculated by ^{1}H NMR, and $Đ$ = 1.03).

2.4. Synthesis of α,ω-Functionalized PI (HO-PI-OH). Isoprene (6.12 g) was added to 120 mL of benzene, followed by the addition of *t*BDMSOPrLi (1.02 mmol), and allowed to polymerize at 40 °C for 24 h. Then, EO (∼1 mL) was added to the reaction mixture and kept for 8 h, and the polymerization was terminated by addition of methanol (<1 mL). The reaction solution was poured into a large excess of methanol, and the precipitated final polymer was dried in a vacuum oven at 40 °C overnight. Finally, a postpolymerization reaction (deprotection of the OH group) was performed under argon to remove the silyl-protecting group. In a round bottom flask, 2 g (0.317 mmol) of the α-protected, ω-functionalized PI-OH was dissolved in 30 mL of dry THF and reacted with an excess of TBAF (3.17 mmol) for 48 h at room temperature (Figure 1b). The THF was removed using a rotary evaporator, and the polymer was redissolved in dichloromethane (CH_2Cl_2, 30 mL). The solution was poured into three times excess of methanol, centrifuged, and dried in a vacuum oven for 24 h.

2.5. Size Exclusion Chromatography. Size exclusion chromatography (SEC) measurements were carried out at 35 °C using a Viscotek GPCmax VE-2001 equipped with an isocratic pump, Styragel HR2, HR4, and HR5 columns in series (300 mm × 8 mm) and a differential refractive index detector with THF as the eluent at a flow rate of 1.0 mL/min. The system was calibrated with

https://doi.org/10.1021/acs.macromol.2c01527
Macromolecules 2022, 55, 10491−10501

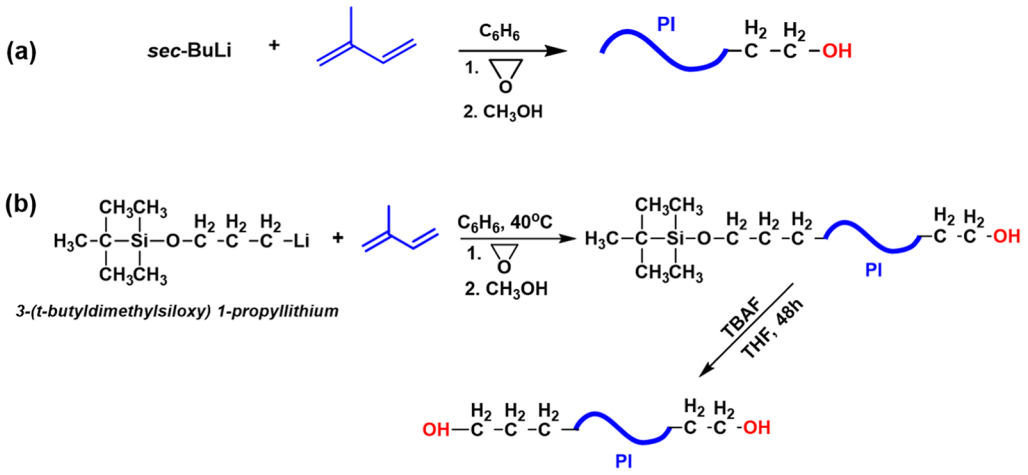

Figure 1. Synthetic procedures for (a) ω-functionalized PI-OH and (b) α,ω-functionalized HO-PI-OH.

1,4-PI standards (M_p: 580 to 1,220,000 g mol^{-1}). The 1,4-content of the PI standards was similar to the synthesized ones (88−92%). SEC measurements led to the calculation of the number average molecular weight (M_n) of the PIs and their dispersity ($Đ$).

2.6. Proton Nuclear Magnetic Resonance Spectroscopy. ^{1}H NMR spectra were recorded on a Bruker AVANCED III spectrometer operating at 500 MHz at room temperature. Chloroform-d ($CDCl_3$) was used as the solvent in all cases. ^{1}H NMR spectra were used to determine the number average molecular weight (M_n) of the synthesized polymers from the integral ratio of the protons of the end group and the characteristic protons of the monomeric units. The 1,4-content in each polymer was also determined.

2.7. Differential Scanning Calorimetry. Differential scanning calorimetry (DSC) with a Q2000 (TA Instruments) equipped with a liquid nitrogen cooling system (LNCS) was employed for the thermal properties of di-functionalized PIs. The temperature protocol involved measurements on cooling and subsequent heating at a rate of 10 K min^{-1} and in a temperature range between 173 and 323 K. The instrument was calibrated for best performance in the specific temperature range and heating/cooling rate. A precalibration procedure included (i) cleaning of the cell, (ii) a cell conditioning step (making an inert atmosphere by employing helium gas), and (iii) a LNCS baseline calibration. The main Tzero calibration sequence included a baseline calibration for the determination of the time constants and capacitances of the sample and reference sensor using a sapphire standard. In the next step, an indium standard (ΔH = 28.71 J/g, T_m = 428.8 K, with a heating rate of 10 K min^{-1}) was employed for the enthalpy and transition temperature calibration. As a final step, an empty cell baseline measurement verified the successful calibration of the instrument. Concerning the heat capacity calibration, a temperature modulated DSC (TM-DSC) calibration was made with a sapphire standard. Samples (typically ≈ 5−6 mg) were hermetically encapsulated in an aluminum Tzero pan and placed on the sample sensor. An empty aluminum pan was used, as a reference.

2.8. Dielectric Spectroscopy. DS measurements were performed with a Novocontrol Alpha frequency analyzer. The temperature stability was controlled by the Quatro system, by employing a nitrogen gas. The temperature protocol of "isobaric" measurements ranged from 173 to 333 K in steps of 5 K (and steps of 2 K in the vicinity of T_g) and for frequencies in the range from 10^{-2} to 10^7 Hz. The samples were stabilized at each temperature (within 0.05 K) for at least 20 min to achieve a thermal equilibration. DS measurements were carried out in the usual parallel plate geometry with electrodes of 20 mm in diameter and a sample thickness of 50 μm was maintained by poly(tetrafluoroethylene) (Teflon) spacers. Before the measurement, the samples were dried in a vacuum oven at 303 K, for ∼12 h. Measurements under hydrostatic pressure were carried out in a Novocontrol pressure cell.[45] The pressure setup consisted of a T-controlled cell and hydraulic closing press with an air pump for hydrostatic test pressure. For the P-dependent measurements, the functionalized polymers were placed between 20 mm electrodes, and Teflon spacers were used to maintain a thickness of 50 μm. Subsequently, the capacitor was wrapped with Teflon tape and placed inside a Teflon ring in order to prevent the flow of silicone oil (Dow Corning 550 Fluid) into the sample. The silicone oil is the liquid that uniformly transmits the pressure to the capacitor. The isothermal measurements of relaxation times were performed with temperature stability better than 0.1 K and pressure stability better than 2 MPa. For T < 295 K, a refrigerated circulator (Julabo FP 40) was employed for the control of temperature stability. Both in "isothermal" and "isobaric" measurements, the complex dielectric permittivity $\varepsilon^* = \varepsilon' - i\varepsilon''$, where ε' is the real and ε'' is the imaginary part, was obtained as a function of frequency, ω, temperature, T, and pressure, P, that is, $\varepsilon^*(T, P, \omega)$.[48,49] The analysis was carried out with the empirical equation of Havriliak and Negami (HN):

$$\varepsilon^*_{HN}(\omega, T, P) = \varepsilon_\infty(T, P) + \sum_{j=1}^{3} \frac{\Delta\varepsilon(T, P)}{[1 + (i\omega\tau_{HN_j}(T, P))^{m_j}]^{n_j}} + \frac{\sigma_0(T, P)}{i\varepsilon_f\omega} \quad (1)$$

where $\varepsilon_\infty(T,P)$ is the high-frequency permittivity, $\tau_{HN}(T,P)$ is the characteristic relaxation time in this equation, $\Delta\varepsilon(T,P) = \varepsilon_0(T,P) - \varepsilon_\infty(T,P)$ is the relaxation strength, m, n (with limits $0.2 < m, mn \leq 1$) describe, respectively, the symmetrical and asymmetrical broadening of the distribution of relaxation times, σ_0 is the dc conductivity, and ε_f is the permittivity of free space. Assuming statistical independence in the frequency domain, a summation of two (or three) HN functions have been employed for the temperature range, where two (or three) relaxation processes coexist within the experimental window. From τ_{HN}, the relaxation time at maximum loss, τ_{max}, is obtained analytically as follows:[50]

$$\tau_{max} = \tau_{HN}\sin^{-1/m}\left(\frac{\pi m}{2(1+n)}\right)\sin^{1/m}\left(\frac{\pi mn}{2(1+n)}\right) \quad (2)$$

In the analysis of the dynamic behavior, we have used the ε'' values at every temperature. Moreover, we employed the principle of time−temperature superposition (tTs) in isothermal dielectric measurements, which allows the frequency ω dependence of the complex $\varepsilon^*(\omega)$ at any temperature to be determined from a measurement at a reference temperature (Figure 1a and Figure S3a) from the "master curve." The shift factors, α_T, were fitted according to the Williams−Landel−Ferry (WLF) equation as follows

$$\log \alpha_T = -\frac{C_1(T - T_r)}{C_2 + (T - T_r)} \quad (3)$$

https://doi.org/10.1021/acs.macromol.2c01527
Macromolecules 2022, 55, 10491−10501

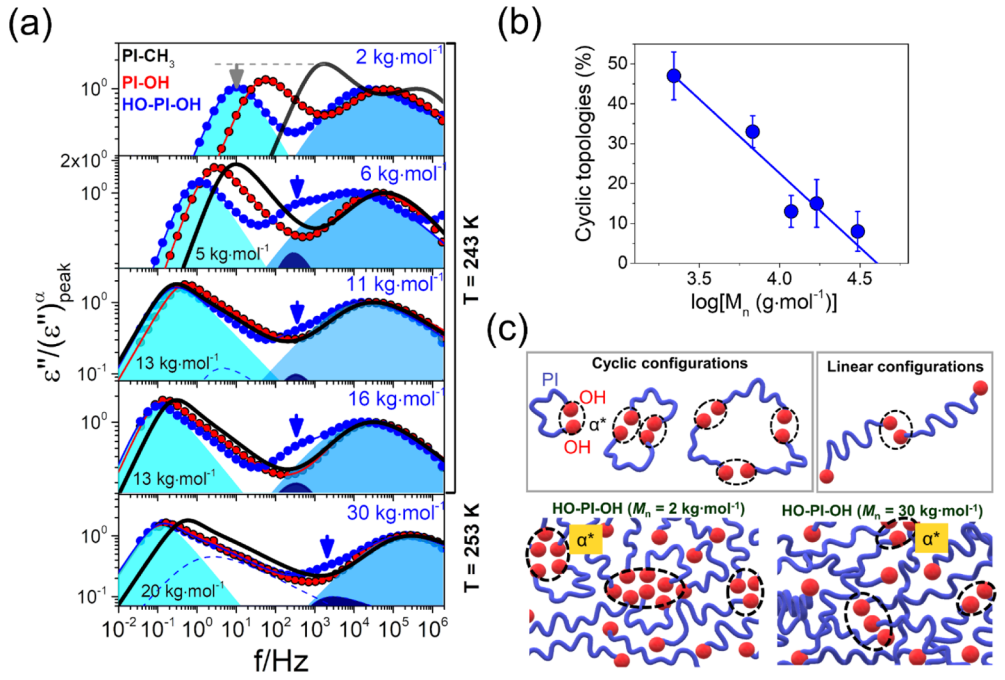

Figure 2. (a) Dielectric loss curves normalized to the peak of the segmental (α) process for PI-CH_3 (black line), PI-OH (red symbols), and HO-PI-OH (blue symbols) with different molar masses as indicated. The shadowed cyan, navy, and blue areas indicate simulations of the longest NM, the α* and α process, respectively. The vertical blue arrows in (a) indicate the "intermediate" (α*) process. (b) Percentage of cyclic topologies as a function of molar mass. (c) Schematic representation of the possible chain configurations in di-functionalized PIs, as well as a schematic representation of chain configurations and h.b. associations at two molar masses: 2 kg mol^{-1} (left) and 30 kg mol^{-1} (right).

where C_1 and C_2 are empirical parameters at the reference temperature (T_r = 243 K, for all molar masses). The WLF coefficients at T_g can be calculated as $c_1^g = c_1^r c_2^r/(c_2^r + T_g - T_r)$ and $c_2^g = c_2^r + T_g - T_r$.

2.9. Rheology. A TA Instruments AR-G2 with a magnetic bearing that allows for nanotorque control was used for recording the viscoelastic properties of the functionalized PIs. Measurements were made with the environmental test chamber as a function of temperature. The samples were prepared on the lower rheometer plate (8 mm); the upper plate was brought into contact, and the sample thickness was adjusted accordingly. Typically, the gap between plates was ~1 mm for all the investigated functionalized PIs. The linear and nonlinear of viscoelastic regions were determined via strain amplitude dependence of the complex shear modulus $|G^*|$ at ω = 10 rad s^{-1}, at each temperature. Subsequently, isothermal frequency sweeps in an angular frequency range of $0.1 < \omega < 100$ rad s^{-1} were carried out in temperature steps of 10 (5) K and with strain amplitudes of ~1% (0.1%) for the higher (close to T_g) temperatures. Before each isothermal measurement, a thermal stabilization of 20 min was employed to ensure thermal equilibrium. Master curves were constructed by using the t*T*s principle. The extracted shift factors, α_T, were fitted according to WLF equation (eq 3). Subsequently, the data were reshifted horizontally (by factors c_T) to achieve iso-friction conditions.

3. RESULTS AND DISCUSSION

3.1. Impact of Hydrogen Bonding on the Chain Configurations and the Associated Molecular Dynamics. Quantitative insight into the impact of h.b. on the topologies and on the segmental and global chain relaxation of mono- and di-functionalized PIs can be obtained from dielectric and rheological measurements. Figure 2a contrasts and compares the dielectric loss curves of methyl-terminated PI, with mono- and di-functionalized PIs with hydroxyl end groups. Systematic differences are evident, especially for the lower molar masses.

As it is anticipated for type-A polymers, the mono-functionalized PIs, as depicted in Figure S3 and in Figure 2, the dielectric and rheological measurements exhibit both the SM and NM. For $M_n \approx 2$ kg mol^{-1}, the slowing down and broadening of the segmental relaxation as well as the reduced chain relaxation strength, as compared to PI-CH_3, reflect the increased h.b. interactions (Figure 2).[38] Evidently, the latter affect the chain configurations and lead to the formation of PI star/flower structures with the polar OH-groups comprising their centers. However, the absence of the arm retraction mechanism (relaxing process of stars[51,52]) (Figure S3b) in the rheological measurements implies that the chains retain their linear configurations, but with increased intermolecular h.b. interactions.[33] Interestingly, for the PI-OH 2 kg mol^{-1}, there is a reduced dielectric strength that, however, cannot arise from cyclic topologies (monofunctional PIs cannot form rings). In this respect, the results from a recent study on the dielectric relaxation behavior of entangled linear type-A polymers undergoing head-to-head association and dissociation are relevant.[53] In general, changes in the dielectric function and a retardation (acceleration) of the dielectric function of the unimer (dimer), respectively, were evidenced because of the pairwise feature of the coupling. For the higher molar masses, there are reduced h.b. due to the reduced concentration of polar end groups. The relaxation map of the mono-functionalized PIs, depicting the local dipole fluctuations into the glassy state (β process), the SM and NM relaxations is provided in Figure S4.

The incorporation of OH-groups at both chain ends is anticipated to strongly affect the molecular dynamics and the chain topologies. The molecular dynamics of the di-functionalized PIs can be discussed with the help of Figure 2, as well as from the molar mass dependence of the superimposed curves obtained from dielectric and rheological measurements (Figure

https://doi.org/10.1021/acs.macromol.2c01527
Macromolecules 2022, 55, 10491−10501

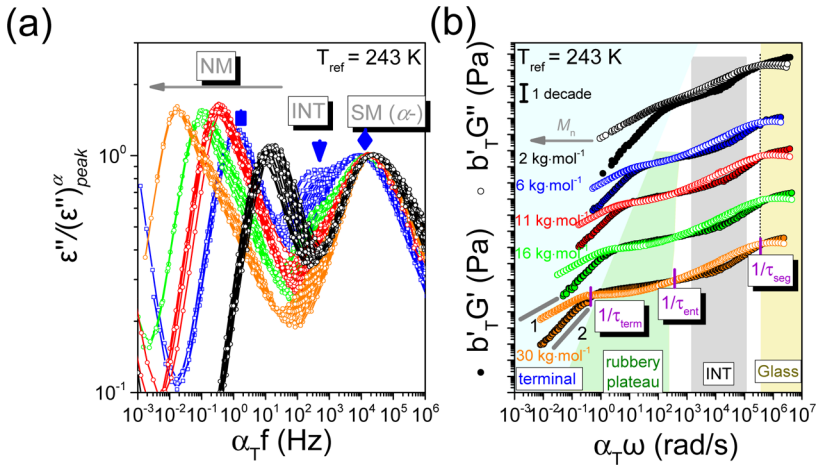

Figure 3. (a) Dielectric loss curves normalized to the peak frequency of the segmental process and further shifted horizontally to the same process, by employing the t*T*s at a reference temperature of 243 K, for di-functionalized PIs. The segmental mode (SM), the intermediate process (INT), and normal mode (NM) are indicated by rhombi, vertical arrow, and square symbols for $M_n \approx 6$ kg mol^{-1}. (b) Superimposed curves of storage (filled symbols) and loss (open symbols) moduli by employing the t*T*s principle at the same reference temperature (243 K). Lines with slopes 1 and 2 are also shown in (b). The yellow, gray, green, and blue areas indicate the glassy region, the frequency range of the dielectric intermediate process, the rubbery plateau and the terminal region, respectively. "Master curves" correspond to different molar masses: 2 kg mol^{-1} (black), 6 kg mol^{-1} (blue), 11 kg mol^{-1} (red), 16 kg mol^{-1} (green), and 30 kg mol^{-1} (orange), obtained on cooling. Curves are shifted vertically for clarity.

3). Parenthetically, a fractional free volume, $f(T_g)$, of ~2.8 (2.8) % and a thermal expansion coefficient of the free volume, α_f, of ~7.1 (8.0) ± 0.4 (0.8) × 10^{-4} K^{-1} can be calculated at T_g for HO-PI-OH (PI-OH), independently of the molar mass, by employing the WLF coefficients (Figures S5 and S6). The rheological measurements of HO-PI-OH exhibit the typical features of amorphous linear polymers. Starting from higher frequencies: (i) the glassy elastic plateau, (ii) crossover of $G'(\omega)$ and $G''(\omega)$ that is accompanied by the structural relaxation peak of $G''(\omega)$ (segmental relaxation, T_g was extracted at the crossing point), (iii) Rouse modes followed by the rubbery plateau for higher molar masses, and (iv) the typical terminal behavior ($G'(\omega) \approx \omega^2$ and $G''(\omega) \approx \omega^1$). Evidently, the presence of the typical terminal relaxation and the absence of a lengthened rubbery plateau (for lower molar masses) rules out the formation of large supramolecular networks that are long-lived. On the other hand, the dielectric loss curves do not obey the t*T*s principle. This reflects the presence of an intermediate process in DS.

Additionally, DS can provide precise information on the presence of cyclic chain configurations in type-A polymers, through the NM relaxation. Specifically, in cyclic type-A polymers, the parallel component of the dipole moment vanishes. This results in the disappearance of the NM relaxation peak for the latter topologies, as has been shown recently for isoregic structures.[54,55]

At this point, a comparison of the NM dielectric strength of the HO-PI-OH with that of PI-OH and with PI-CH_3 is informative (Figure 3). The reduced NM dielectric strength of HO-PI-OH, as compared to mono- (and methyl-terminated) PIs, reveals a mixture of linear and cyclic configurations (Figure 2a) in the former. The latter can be formed via the interactions of −OH groups located within the same chain or in different chains, as depicted in Figure 2c. From the plausible cyclic configurations of Figure 2c, the ones that more effectively reduce the dielectric strength are associations within a single chain (the dipoles of two or more associated chains can be aligned in a way that are still dielectrically active). The content of cyclic configurations, X_{cyclic}, can be determined by the reduced dielectric strength of the NM as $X_{cyclic} = 1 - \left[\frac{(\Delta\varepsilon_{max})_{NM}^{HO-PI-OH}}{(\Delta\varepsilon_{max})_{NM}^{PI-CH3}}\right]$, after the normalization to the maximum of the α process. X_{cyclic} increases significantly by decreasing molar mass from 2 to 30 kg mol^{-1}, as a result of the increasing concentration of polar end groups (Figure 2c). An estimated ~45% cyclic topologies were found in HO-PI-OH with $M_n \approx 2$ kg mol^{-1}.

The presence of a mixture of linear/cyclic configurations is expected to affect the molecular dynamics due to the lack of free chain ends in the latter configurations. A three-dimensional representation of the temperature and frequency dependence of the dielectric loss curves of HO-PI-OH with $M_n \approx 2$ kg mol^{-1} is provided in Figure S7. Specifically, the shape of the global chain dynamics exhibits the typical terminal behavior with a low-frequency slope, $m = 1$ (i.e., $\varepsilon'' \approx \omega$). The existence of internal Rouse modes in DS curves requires an additional HN function, for higher molar masses, similarly to methyl-terminated PIs (Figure 2). On the other hand, the segmental process exhibits a broader distribution of relaxation times ($\langle m \rangle = 0.6 \pm 0.1$, $\langle mn \rangle = 0.35 \pm 0.01$, for $M_n \approx 6$ kg mol^{-1}), as compared to the NM. In contrast to methyl terminated PIs, the relaxation time of the segmental process remains unaffected from the chain length (molar mass) (Figures 2 and 3a).

Noticeably, an additional process can be observed for the di-functionalized PIs with a narrower distribution of relaxation times ($m \approx 1 \pm 0.01$ and $mn \approx 0.75 \pm 0.01$, for $M_n \approx 6$ kg mol^{-1}) and reduced dielectric strength (by about five times), as compared to the α-relaxation. Parenthetically, for $M_n = 2$ kg mol^{-1}, there is a merge of the α and "intermediate" process resulting to a broader distribution of relaxation times as compared to the respective methyl-terminated PI. The "intermediate" process resembles that found in P(S-*b*-I) copolymers as well as in amine-terminated and carboxylic acid-terminated di-functionalized PDMS.[43] We report on its molecular origin below by employing a combination of *T*- and *P*-dependent dielectric measurements.

https://doi.org/10.1021/acs.macromol.2c01527
Macromolecules 2022, 55, 10491−10501

3.2. Origin of the "Intermediate" Process. The temperature dependence of the extracted relaxation times at maximum loss for the "intermediate" process, as well as for all dielectrically active processes (NM, α and β) in HO-PI-OH polymers having molar masses ranging from 2 to 30 kg mol^{-1} (see Table 1), is depicted in Figure 4.

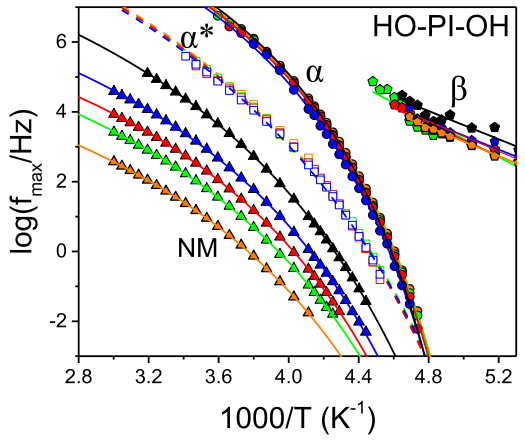

Figure 4. Relaxation map depicting the β (rhombi), α (circles), α* (squares), and the most intense chain process (NM, uptriangles) in di-functionalized PIs with different molar masses: 2 kg mol^{-1} (black), 6 kg mol^{-1} (blue), 11 kg mol^{-1} (red), 16 kg mol^{-1} (green), and 30 kg mol^{-1} (orange). The curved and straight lines represent fits to VFT (eq 4) and Arrhenius equations, respectively.

Starting from lower temperatures, the β process, associated with local dipole fluctuations into the glassy state, exhibits an Arrhenius temperature dependence ($f_{max} = f_\infty \exp(-E/RT)$, with an activation energy of 41 ± 2 kJ mol^{-1}, for $M_n \approx 6$ kg mol^{-1}). At higher temperatures, the intermediate (α*) process together with the SM (α process) and the longest NM conform to the usual Vogel−Fulcher−Tammann (VFT) equation:

$$f_{max} = f_\infty \exp\left(-\frac{B}{T - T_0}\right) \quad (4)$$

where f_∞ is the characteristic frequency in the limit of very high temperatures, B is the activation parameter, and T_0 is the "ideal" glass temperature located below the conventional T_g. The VFT parameters are provided in Table 2. The intermediate process (i) exhibits a strong temperature dependence and (ii) freezes at a temperature in the vicinity to the liquid-to-glass temperature (Table 2). Moreover, it is insensitive to the HO-PI-OH chain length. Therefore, it is provisionally assigned to a segmental-type relaxation and is termed α*.

Alternatively, the α* process could be related to the proposed chain-end association/dissociation process discussed in several h.b. systems.[24,25,29] In this view, the difference in time scales of the α and α* processes defines a characteristic chain-end dissociation energy, E_a, as follows:

$$f_{a*}(T) = f_a(T)\exp\left(-\frac{E_a}{RT}\right) \quad (5)$$

Using the VFT parameters of the α and the α* process (Table 2), we obtain E_a = 9.3 ± 0.2 kJ mol^{-1} (at T = 250 K), that is, about 5 × $k_B T$ which is a reasonable estimate for the strength of h.b. However, the mere presence of the NM process rules out this possibility. In addition, we provide arguments in favor of a new segmental process of those segments located in the vicinity of h.b. (see pressure results below).

Quantitative insight into the molecular origin of the α* process can be obtained by P-dependent dielectric measurements. To this end, we employ the pressure sensitivity of relaxation times and the pressure coefficient of the respective T_g. To the best of our knowledge, it is the first time that the P-dependence of the α* process is investigated in end-functionalized polymers. The ideal molar mass in this endeavor is the $M_n \approx 6$ kg mol^{-1}, due to the high amount (~35%) of cyclic configurations.

By applying pressure, the α and α* processes approach each other, implying that the former exhibits a stronger pressure sensitivity (Figure 5a). The pressure dependence of relaxation times for the two α processes follows the pressure equivalent of VFT equation as follows:[56]

$$f_{max} = f_\infty \exp\left(-\frac{D_P P}{P_0 - P}\right) \quad (6)$$

where f_∞ is the characteristic frequency at atmospheric pressure at a given temperature, D_P is a dimensionless parameter, and P_0 is the pressure corresponding to the "ideal" glass. The D_p value was held fixed to 19.3 (15) for the α (α*) process from a free fit to the 255 K data set. On the other

Table 2. VFT Parameters for the α and α* Processes, Glass Temperature, and Fragility for Di-Functionalized HO-PI-OH with Different Chain Lengths

M_n (g·mol^{-1})	log(f_∞/Hz)	B (K)	T_0 (K)	T_g (K)[a]	T_g (K)[b]	m*
			α Process			
2200	−12*	1202 ± 8	174.5 ± 0.3	209.8 ± 0.3	215.7 ± 0.3	88 ± 2
6800	−12	1290 ± 10	171.9 ± 0.4	209.8 ± 0.4	215.3 ± 0.4	82 ± 3
11800	−12	1257 ± 7	172.3 ± 0.3	208.9 ± 0.3	214.8 ± 0.3	84 ± 2
17000	−12	1277 ± 4	171.2 ± 0.2	208.6 ± 0.2	214.5 ± 0.2	83 ± 1
30600	−12	1257 ± 4	171.5 ± 0.2	208.4 ± 0.2	214.2 ± 0.2	84 ± 1
			Intermediate (α*) Process			
6800	−12	2120 ± 20	148 ± 1	210 ± 1	219 ± 1	50 ± 2
11800	−12	2070 ± 40	150 ± 2	210 ± 2	220 ± 2	52 ± 5
17000	−12	2080 ± 20	148.7 ± 0.7	209.4 ± 0.7	219.0 ± 0.7	51 ± 2
30600	−12	2030 ± 30	151 ± 1	210 ± 1	220 ± 1	53 ± 3

*Held fixed. [a]At τ = 100 s. [b]At τ = 1 s.

https://doi.org/10.1021/acs.macromol.2c01527
Macromolecules 2022, 55, 10491−10501

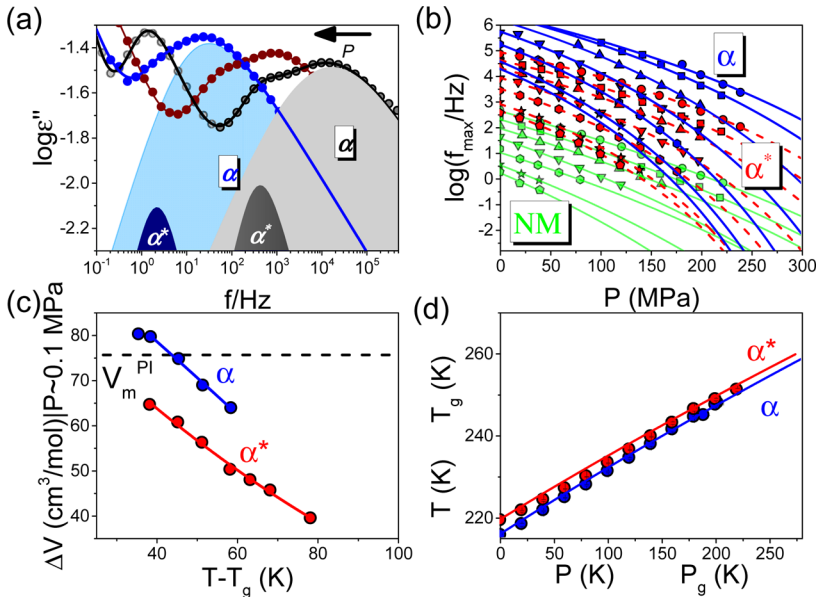

Figure 5. (a) Dielectric loss curves for the HO-PI-OH with M_n = 6 kg mol^{-1}, as a function of frequency under isothermal conditions at T = 248 K. Pressure increases in the direction of the arrow; 20 MPa (gray circles), 80 MPa (red circles), and 140 MPa (blue circles). The respective solid lines (colored areas) represent fits (simulations) to Havriliak−Negami function for the respective processes. (b) Pressure dependence of the characteristic frequencies at maximum loss for the α (blue symbols), α* (red symbols), and longest NM (green symbols) process, at some selected temperatures: 245 K (pentagons), 248 K (stars), 255 K (hexagons), 261 K (down-triangles), 268 K (uptriangles), 273 K (squares), and 278 K (circles). The solid (dashed) lines are fits to eq 6 for the α (α*) process, respectively. (c) Temperature dependence of the apparent activation volume of the α (blue circles) and the α* process (red circles). The horizontal black line represents the repeat unit volume of PI. (d) Pressure dependence of T_gs corresponding to the freezing of the α and α* processes at a characteristic time of τ = 1 s. The solid lines represent fits to the empirical equation for the pressure dependence (see text).

hand, the temperature dependence of the dielectrically active segmental processes under "isobaric" conditions is depicted in Figure S8, following the usual VFT equation (eq 4). The VFT parameters under "isothermal" and "isobaric" conditions are listed in Table S2.

The molecular volume necessary for a specific molecular motion is engraved in the apparent activation volume, $\Delta V^{\#}$. The latter quantity can be calculated explicitly from the pressure sensitivity of relaxation times as $\Delta V^{\#} = 2.303\ RT(\partial \log \tau/\partial P)_T$.[19−21,57,58] The T-dependence of $\Delta V^{\#}$ at ambient pressure is depicted in Figure 5c. The apparent activation volume for the α process exhibits a strong T-dependence, in the vicinity of T_g, approaching the repeat unit of PI at about 50 K above T_g, in accordance with the pressure results of methyl-terminated PIs.[16−18] On the other hand, $\Delta V^{\#}$, for the α* process is somewhat lower, implying a process of the same origin (segmental) but with a lower degree of cooperativity.

Additional information on the molecular origin of the α* process can be obtained from the pressure coefficient of T_g. The $T_g(P)$ corresponding to the α and α* processes are discussed with respect to Figure 5d. The extracted T_gs exhibit qualitatively similar pressure dependence, which can be described by the following empirical equation $T_g(P) = T_g(0)(1 + (\kappa P/\lambda)^{1/\kappa}$.[59] Here, $T_g(0)$ is the T_g at ambient pressure, κ and λ are polymer specific parameters (with values κ = 2 (held fixed), and λ = 1280 ± 10 (1370 ± 30) for the α (α*) process). Specifically, the pressure coefficient of T_g^{α} ($T_g^{\alpha*}$) in the limit of ambient pressure, $dT_g/dP|_{P\to 0}$, is 167 K GPa^{-1} (160 K GPa^{-1}), similar to that found in methyl-terminated PI ($dT_g/dP|_{P\to 0}$ = 180 ± 20 K GPa^{-1}).[57] Moreover, as depicted in Figure S9, the dielectric strength of the NM with respect to the segmental (α) process, increases with increasing pressure, indicating the breaking of h.b. Evidently, the P-dependent results together with T-dependent dielectric data support the notion that the α* process is a segmental-type process associated with the localized regions of increased friction in the vicinity of the polar end-groups (see Figure 2c).

3.3. Impact of Hydroxyl End-Group Functionalization on Molecular Dynamics. The molar mass dependence of the two dielectric T_gs can be discussed with respect to Figure 6. Parenthetically, the thermodynamic (DSC) measurements

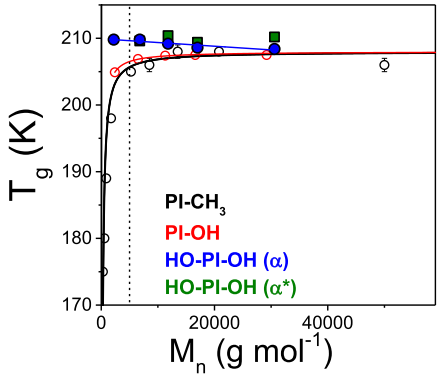

Figure 6. (a) Molar mass dependence of the liquid-to-glass temperature for the mono-functionalized (red symbols) and the di-functionalized (blue symbols). The glass temperatures extracted from the α* process in the di-functionalized polymers are also included (in green). The glass temperature is operationally defined as the temperature where the dielectric loss maximum of the segmental process is at 100 s. Data from methyl-terminated PIs (black symbols) are also included for comparison.[60,61] The black solid line is a fit to the Fox−Flory equation.

https://doi.org/10.1021/acs.macromol.2c01527
Macromolecules 2022, 55, 10491−10501

display a single step signifying a single liquid-to-glass temperature. This is possibly a result of (i) the proximity of the two T_gs and (ii) the small size of the cooperative domains (Figure S10).[44]

The glass temperature of the methyl-terminated and monofunctionalized PIs conforms to the Fox–Flory equation, $T_g(M_w) = T_g^{\infty} - A/M_w$, where, T_g^{∞} (208 K for both mono- and nonfunctionalized PIs), is the glass temperature in the limit of very high molar masses and A (= 11700 ± 900 g K mol^{-1}, for PI-CH$_3$, and 7500 ± 300 for PI-OH) is a fitting parameter. For the monofunctionalized PIs, there is a slight increase of T_g for the lower molar masses, indicating increased h.b. interactions.[38] The T_g (corresponding to the α process) of di-functionalized PIs remains almost independent of molar mass. This situation for HO-PI-OH is reminiscent to that found for cyclic polystyrenes (c-PS), despite the lower content (up to 45%) of cyclic topologies in the present system.[62] A similar molar mass dependence of T_g was evidenced in di-functionalized PPG with hydroxyl end-groups.[35] Conversely, an increasing T_g with decreasing molar mass was evidenced in HO-PDMS-OH.[35,42,43] These observations were discussed by the difference in lifetime of the end-group associations relative to the segmental and chain relaxation times. In all the investigated cases, hydrogen-bonded end groups restrict the backbone mobility and increase T_g. In linear polymers without specific interactions at the chain ends, the decrease of T_g with decreasing molar mass reflects the faster backbone dynamics by the mobile free ends. It is worth noting that the freezing of the segments in the vicinity of hydrogen-bonded regions (α* process) exhibits a similar molar dependence with the conventional liquid-to-glass transition (α process), reflecting the strong impact of h.b. on both segmental relaxations.

To quantify and compare the temperature dependence of the α and α* relaxation times in the vicinity of the respective T_gs, we employ the steepness index (fragility), m defined as $\partial \log \tau/\partial(T_g/T)|_{T=Tg}$, which is equivalent to the slope in the "fragility" plot of log τ versus T_g/T.[63] The steepness index can readily be calculated as $m^* = BT_g/[2.303(T_g - T_0)^2]$.[63] The fragilities obtained from the two processes are almost independent of molar mass (Figure S11). The extracted fragility for the a process is similar to PI-OH and slightly higher than that of PI-CH$_3$, in accordance with the literature results for h.b. systems.[35,42,43] However, the fragility for the a* process ($\langle m_{a^*}\rangle$= 52 ± 1, at τ = 100 s) is significantly lower in comparison to the segmental process $\langle m_a\rangle$ = 83 ± 1 (Figure S11).[64,65]

A comparison of the rheological and the dielectric master curves for the di-functionalized PI with a molar mass of 30 kg mol^{-1} is provided in Figure 7. Respective data for a molar mass of 6 kg mol^{-1} are provided in Figure S12.

The peak frequency of the "intermediate" dielectric process is located between the segmental process and the process associated with the relaxation of a single entanglement strand ($1/\tau_e$) in rheology, pointing toward a sub-Rouse process (a localized, segmental-type process) (Figure S12).[22,23] For di-functionalized PIs, there is a failure of tTs both in DS and in rheology reflecting the presence of α* process. The latter is more evident by examining the loss tangent (tan δ). Moreover, an estimation of the entanglement molar mass, M_e (=$4\rho RT/5G_N^0$) can be obtained from the plateau modulus, G_N^0 (~0.29 MPa). Employing a density of 0.88 g mol^{-1}, at 243 K, an entanglement molar mass, $M_e \approx$ 4900 g mol^{-1} was calculated

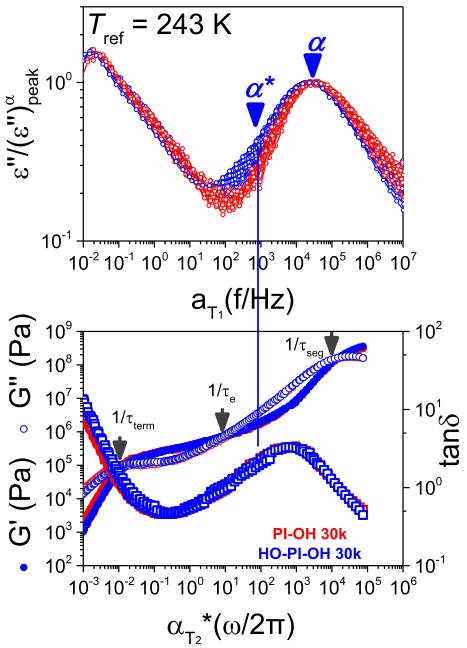

Figure 7. Comparison of the superimposed curves of (top) the dielectric loss with the master curves of (bottom) the storage (filled circles) and loss (open circles) moduli, as well as tan δ (open squares) of PI-OH (red symbols) and HO-PI-OH (blue symbols) with a molar mass of 30 kg mol^{-1}, all at the same reference temperature of 243 K. Vertical solid line gives the characteristic frequency of the α* process. In rheology, the vertical arrows indicate the inverse time of the segmental process (τ_{seg}), the Rouse time of an entanglement strand (τ_e), and the terminal time (τ_{term}).

for di-functionalized PIs. It is almost identical to that of PI-OH and PI-CH$_3$ analogues ($M_e \approx$ 5000 g mol^{-1}).

The entanglement molar mass, M_e, can be also estimated by the molar mass dependence of normalized most intense chain mode relaxation times reduced by the corresponding segmental mode from a log–log representation, as shown in Figure 8a.

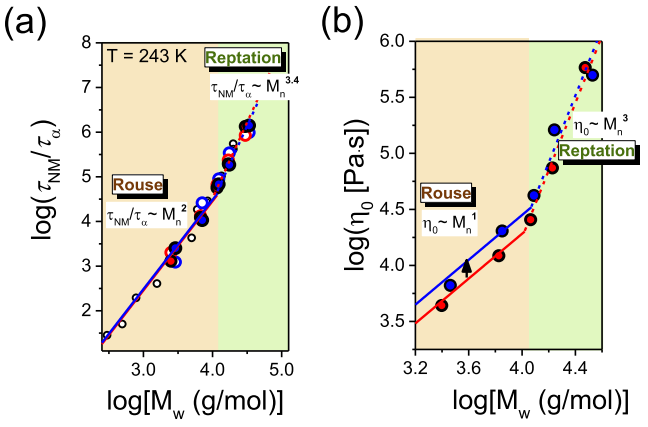

Figure 8. Molar mass dependence of (a) longest normal mode times normalized by the corresponding segmental times and (b) zero-shear viscosity, for PI-OH (red symbols) and HO-PI-OH (blue symbols) plotted in a log–log representations at the reference temperature (243 K). Literature data[60,61] for PI-CH$_3$ also included in (a) (black circles) for comparison. The red (blue) solid and dashed lines represent linear fits into the Rouse and reputation regime, respectively, for HO-PI-OH (PI-OH).

https://doi.org/10.1021/acs.macromol.2c01527
Macromolecules 2022, 55, 10491–10501

The zero shear viscosities, $\eta_0 = \lim_{\omega\to 0}[|\eta^*(\omega)|]$, of the di-functionalized and monofunctionalized PIs can be compared for each molar mass (Figure S13). Considering the dependence of T_g on the molar mass (especially for the monofunctionalized PIs), the master curves were horizontally shifted to the SM. In accordance with the predictions of the Rouse (reptation) model, the zero-shear viscosity scales as $\eta_0 \approx M^1$ ($\eta_0 \approx M^{3.4}$), for lower (higher) molar masses with a critical molecular weight, $M_c \approx 12500$ (11400) g mol^{-1} for the HO-PI-OH (PI-OH). Specifically, a ratio $M_c/M_e \approx 2.5$ can be extracted for di-functionalized PIs, similar to that found in methyl-terminated PI (70% cis).[66,67] In the case of cyclic polymers, a molar mass dependence of zero shear viscosity as $\eta_0 \approx N^{1.4\pm0.2}$ is anticipated.[68−70] However, the present di-functionalized PIs are mixtures of cyclic topologies and of linear chains. It has been well documented in literature that even a small amount of linear "contaminants" in cyclic topologies strongly affects the terminal relaxation that becomes indistinguishable from their linear analogues.[68] On the other hand, in going from the mono-to di-functionalized PIs, the absolute value of zero shear viscosity increased for the lower molar masses. A similar trend was evidenced in end-functionalized PDMS,[42,43] in polyglycerol,[71] as well as in linear polymers functionalized by strong stickers in the middle of the chains.[72] The increased zero-shear viscosity for the unentangled chains in the linear/cyclic mixtures can be discussed by the presence of increased h.b. interactions, and the increased T_gs of the cyclic topologies (Figure 6). Lastly, we refer to a recent study of the viscoelastic behavior of linear and ring Rouse chains undergoing reversible end-association and dissociation.[73] It was shown that the terminal viscoelastic relaxation processes of the cyclic and linear chains are slower and faster than respective pure Rouse processes when the motional coupling due to the reaction was significant for both chains.

Overall, the combination of low molar mass polymers (M_n < 2 kg mol^{-1}) with functional hydroxyl end-groups can significantly increase the h.b. interactions and result to systems with a high proportion of cyclic topologies (>45%). The percentage of cyclic topologies can be further tuned by selecting end-groups with even stronger interactions. Importantly, type-A polymers allow for a quantitative estimation of the amount of cyclic topologies by employing DS.

4. CONCLUSIONS

The impact of hydroxyl functionalization at the chain end(s) of linear PIs on the chain configuration and the associated molecular dynamics was studied by means of DS and rheology. DS identified a mixture of linear and cyclic configurations in the di-functionalized PIs. From the reduced strength of the chain modes in DS, the percentage of cyclic topologies could be estimated. It was shown that cyclic topologies can comprise about half of topologies for the lower molar masses. Cyclic configurations impacted all the dynamic properties. Distinctly different from linear polymers, the glass temperature was nearly independent of molar mass for the lower molar masses. Moreover, an additional process (termed α^*) showed up for the di-functionalized PIs in the range between the longest normal mode and the segmental α process, leading to a failure of tTs both in DS and in rheology. By employing the pressure sensitivity of the characteristic relaxation times and the pressure dependence of T_g, we concluded that the α^* process is likely to be associated with the relaxation of segments in the vicinity of h.b. groups, that is, segments having increased friction. As a segmental-type process, the α^* follows a VFT temperature dependence and freezes at a temperature in the vicinity of the liquid-to-glass temperature.

On the other hand, the terminal relaxation and the entanglement molar mass were reminiscent to that of methyl-terminated or mono-functionalized PIs because the viscoelastic properties of cyclic/linear mixtures are governed by the linear topologies. Nevertheless, the absolute value of zero shear viscosity increased for the lower molar masses in di-functionalized PIs, reflecting the increased h.b. interactions.

This study provides quantitative insight into the molecular dynamics of functionalized type-A polymers bearing weak associating (hydroxyl) end-groups. Furthermore, it provides promising routes toward the design of polymers with a higher content of cyclic configurations. The latter can be achieved by employing low molar masses (M_n < 2 kg mol^{-1}) and well-defined end-functionalized polymers with strongly associating end groups (like zwitterionic groups).

■ ASSOCIATED CONTENT

Supporting Information

The Supporting Information is available free of charge at https://pubs.acs.org/doi/10.1021/acs.macromol.2c01527.

Molecular characteristics (SEC and ^{1}H NMR), additional DSC, dielectric, and rheological data for HO-PI-OH and PI-OH functionalized polymers (PDF)

■ AUTHOR INFORMATION

Corresponding Authors

Nikos Hadjichristidis − *Polymer Synthesis Laboratory, KAUST Catalysis Center, Physical Sciences and Engineering Division, King Abdullah University of Science and Technology (KAUST), Thuwal 23955, Saudi Arabia;* orcid.org/0000-0003-1442-1714; Email: nikolaos.hadjichristidis@kaust.edu.sa

George Floudas − *Department of Physics, University of Ioannina, Ioannina 451 10, Greece; University Research Center of Ioannina (URCI)—Institute of Materials Science and Computing, 451 10 Ioannina, Greece;* orcid.org/0000-0003-4629-3817; Email: gfloudas@uoi.gr

Authors

Achilleas Pipertzis − *Department of Physics, University of Ioannina, Ioannina 451 10, Greece*

Konstantinos Ntetsikas − *Polymer Synthesis Laboratory, KAUST Catalysis Center, Physical Sciences and Engineering Division, King Abdullah University of Science and Technology (KAUST), Thuwal 23955, Saudi Arabia;* orcid.org/0000-0002-9236-931X

Complete contact information is available at: https://pubs.acs.org/10.1021/acs.macromol.2c01527

Notes

The authors declare no competing financial interest.

■ ACKNOWLEDGMENTS

This research was supported by the Hellenic Foundation for Research and Innovation (H.F.R.I.) under the "First Call for H.F.R.I. Research Projects to support Faculty members and Researchers and the procurement of high-cost research equipment grant" (project number: 183). A.P. was financially

supported by the program "PERIFEREIAKI ARISTEIA" (Regional Excellence) cofinanced by the European Union and the Hellenic Republic Ministry of development and investments under NSRF 2014−2020 (Region of Epirus, call 111). K.N. and N.H. would like to acknowledge the support of King Abdullah University of Science and Technology (KAUST).

REFERENCES

(1) Aida, T.; Meijer, E. W.; Stupp, S. I. Functional Supramolecular Polymers. *Science* **2012**, *335*, 813−817.
(2) Brunsveld, L.; Folmer, B. J. B.; Meijer, E. W.; Sijbesma, R. P. Supramolecular Polymers. *Chem. Rev.* **2001**, *101*, 4071−4098.
(3) Akelah, A.; Moet, A. *Functionalized Polymers and Their Applications*; Chapman and Hall: London, 1990.
(4) Yang, L.; Tan, X.; Wang, Z.; Zhang, X. Supramolecular Polymers: Historical Development, Preparation, Characterization, and Functions. *Chem. Rev.* **2015**, *115*, 7196−7239.
(5) Hadjichristidis, N.; Pispas, S.; Pitsikalis, M. End-functionalized Polymers with Zwitterionic End-groups. *Prog. Polym. Sci.* **1999**, *24*, 875−915.
(6) Prins, L. J.; Reinhoudt, D. N.; Timmerman, P. Noncovalent Synthesis Using Hydrogen Bonding. *Angew. Chem., Int. Ed.* **2001**, *40*, 2382−2426.
(7) Zhou, D.; Zhu, L.-W.; Wu, B.-H.; Xu, Z.-K.; Wan, L.-S. End-Functionalized Polymers by Controlled/Living Radical Polymerizations: Synthesis and Applications. *Polym. Chem.* **2022**, *13*, 300−358.
(8) Webber, M. J.; Appel, E. A.; Meijer, E. W.; Langer, R. Supramolecular Biomaterials. *Nat. Mater.* **2015**, *15*, 13−26.
(9) Xie, T. Tunable Polymer Multi-Shape Memory Effect. *Nature* **2010**, *464*, 267−270.
(10) Lo Verso, F.; Likos, C. N. End-Functionalized Polymers: Versatile Building Blocks for Soft Materials. *Polymer* **2008**, *49*, 1425−1434.
(11) Adachi, K.; Kotaka, T. Dielectric Normal Mode Relaxation. *Prog. Polym. Sci.* **1993**, *18*, 585−622.
(12) Schönhals, A. Relation Between Main and Normal Mode Relaxations for Polyisoprene Studied by Dielectric Spectroscopy. *Macromolecules* **1993**, *26*, 1309.
(13) Plazek, D. J.; Schlosser, E.; Schönhals, A.; Ngai, K. L. Breakdown of the Rouse Model for Polymers Near the Glass Transition Temperature. *J. Chem. Phys.* **1993**, *98*, 6488−6491.
(14) Watanabe, H. Dielectric Relaxation of Type-A Polymers in Melts and Solutions. *Macromol. Rapid Commun.* **2001**, *22*, 127−175.
(15) Boese, D.; Kremer, F. Molecular Dynamics in Bulk cis-Polyisoprene as Studied by Dielectric Spectroscopy. *Macromolecules* **1990**, *23*, 829.
(16) Floudas, G.; Meramveliotaki, K.; Hadjichristidis, N. Segmental and Chain Dynamics of Polyisoprene in Block Copolymer/Homopolymer Blends. A Dielectric Spectroscopy Study. *Macromolecules* **1999**, *32*, 7496−7503.
(17) Floudas, G.; Hadjichristidis, N.; Iatrou, H.; Pakula, T. Microphase Separation in Model 3-Miktoarm Star Co- and Terpolymers. 2. Dynamics. *Macromolecules* **1996**, *29*, 3139.
(18) Fukao, K. Dynamics in Thin Polymer Films by Dielectric Spectroscopy. *Eur. Phys. J. E: Soft Matter Biol. Phys.* **2003**, *12*, 119.
(19) Floudas, G.; Gravalides, C.; Reisinger, T.; Wegner, G. Effect of Pressure on the Segmental and Chain Dynamics of Polyisoprene. Molecular Weight Dependence. *J. Chem. Phys.* **1999**, *111*, 9847.
(20) Floudas, G.; Reisinger, T. Pressure Dependence of the Local and Global Dynamics of Polyisoprene. *J. Chem. Phys.* **1999**, *111*, 5201−5204.
(21) Pawlus, S.; Alexei, P.; Sokolov, A. P.; Paluch, M.; Mierzwa, M. Influence of Pressure on Chain and Segmental Dynamics in Polyisoprene. *Macromolecules* **2010**, *43*, 5845−5850.
(22) Spyridakou, M.; Maji, T.; Gkikas, M.; Ngai, K. L.; Floudas, G. Sub-Rouse Dynamics in Poly(isobutylene) as a Function of Molar Mass. *Macromolecules* **2021**, *54*, 9091−9099.
(23) Paluch, M.; Pawlus, S.; Sokolov, A. P.; Ngai, K. L. Sub-Rouse Modes in Polymers Observed by Dielectric Spectroscopy. *Macromolecules* **2010**, *43*, 3103−3106.
(24) Leibler, L.; Rubinstein, M.; Colby, R. H. Dynamics of Reversible Networks. *Macromolecules* **1991**, *24*, 4701−4707.
(25) Rubinstein, M.; Semenov, A. N. Thermoreversible Gelation in Solutions of Associating Polymers. 2. Linear Dynamics. *Macromolecules* **1998**, *31*, 1386−1397.
(26) Rubinstein, M.; Semenov, A. N. Dynamics of Entangled Solutions of Associating Polymers. *Macromolecules* **2001**, *34*, 1058−1068.
(27) Feldman, K. E.; Kade, M. J.; Meijer, E. W.; Hawker, C. J.; Kramer, E. J. Model Transient Networks from Strongly Hydrogen-Bonded Polymers. *Macromolecules* **2009**, *42*, 9072−9081.
(28) Stukalin, E. B.; Cai, L.-H.; Kumar, N. A.; Leibler, L.; Rubinstein, M. Self-Healing of Unentangled Polymer Networks with Reversible Bonds. *Macromolecules* **2013**, *46*, 7525−7541.
(29) Chen, Q.; Tudryn, G. J.; Colby, R. H. Ionomer Dynamics and the Sticky Rouse Model. *J. Rheol.* **2013**, *57*, 1441.
(30) Fetters, L. J.; Graessley, W. W.; Hadjichristidis, N.; Kiss, A. D.; Pearson, D. S.; Younghouse, L. B. Association Behavior of End-Functionalized Polymers. 2. Melt Rheology of Polyisoprenes with Carboxylate, Amine, and Zwitterion End Groups. *Macromolecules* **1988**, *21*, 1644.
(31) van Ruymbeke, E.; Vlassopoulos, D.; Mierzwa, M.; Pakula, T.; Charalabidis, D.; Pitsikalis, M.; Hadjichristidis, N. Rheology and Structure of Entangled Telechelic Linear and Star Polyisoprene Melts. *Macromolecules* **2010**, *43*, 4401−4411.
(32) Vlassopoulos, D.; Pitsikalis, M.; Hadjichristidis, N. Linear Dynamics of End-Functionalized Polymer Melts: Linear Chains, Stars, and Blends. *Macromolecules* **2000**, *33*, 9740−9746.
(33) Kow, C.; Morton, M.; Fetters, L. J.; Hadjichristidis, N. Glass Transition Behavior of Polyisoprene: The influence of Molecular Weight, Terminal Hydroxy Groups, Microstructure, and Chain Branching. *Rubber Chem. Technol.* **1982**, *55*, 245−252.
(34) Roland, C. M. Terminal and Segmental Relaxations in Epoxidized Polyisoprene. *Macromolecules* **1992**, *25*, 7031−7036.
(35) Xing, K.; Tress, M.; Cao, P.-F.; Fan, F.; Cheng, S.; Saito, T.; Sokolov, A. P. The Role of Chain-End Association Lifetime in Segmental and Chain Dynamics of Telechelic Polymers. *Macromolecules* **2018**, *51*, 8561−8573.
(36) Kaminski, K.; Kipnusu, W. K.; Adrjanowicz, K.; Mapesa, E. U.; Iacob, C.; Jasiurkowska, M.; Wlodarczyk, P.; Grzybowska, K.; Paluch, M.; Kremer, F. Comparative Study on the Molecular Dynamics of a Series of Polypropylene Glycols. *Macromolecules* **2013**, *46*, 1973−1980.
(37) Yan, T. Z.; Schröter, K.; Herbst, F.; Binder, W. H.; Thurn-Albrecht, T. Nanostructure and Rheology of Hydrogen-Bonding Telechelic Polymers in the Melt: From Micellar Liquids and Solids to Supramolecular Gels. *Macromolecules* **2014**, *47*, 2122−2130.
(38) Yan, T. Z.; Schröter, K.; Herbst, F.; Binder, W. H.; Thurn-Albrecht, T. Unveiling the Molecular Mechanism of Self-Healing in a Telechelic, Supramolecular Polymer Network. *Sci. Rep.* **2016**, *6*, 32356.
(39) Yan, T. Z.; Schröter, K.; Herbst, F.; Binder, W. H.; Thurn-Albrecht, T. What Controls the Structure and the Linear and Nonlinear Rheological Properties of Dense, Dynamic Supramolecular Polymer Networks? *Macromolecules* **2017**, *50*, 2973−2985.
(40) Mordvinkin, A.; Döhler, D.; Binder, W. H.; Colby, R. H.; Saalwächter, K. Rheology, Sticky Chain, and Sticker Dynamics of Supramolecular Elastomers Based on Cluster-Forming Telechelic Linear and Star Polymers. *Macromolecules* **2021**, *54*, 5065−5076.
(41) Lund, R.; Plaza-García, S.; Alegría, A.; Colmenero, J.; Janoski, J.; Chowdhury, S. R.; Quirk, R. P. Polymer Dynamics of Well-Defined, Chain-End-Functionalized Polystyrenes by Dielectric Spectroscopy. *Macromolecules* **2009**, *42*, 8875−8881.

https://doi.org/10.1021/acs.macromol.2c01527
Macromolecules 2022, 55, 10491−10501

(42) Xing, K.; Chatterjee, S.; Saito, T.; Gainaru, C.; Sokolov, A. P. Impact of Hydrogen Bonding on Dynamics of Hydroxyl-Terminated Polydimethylsiloxane. *Macromolecules* **2016**, *49*, 3138−3147.
(43) Xing, K.; Tress, M.; Cao, P.; Cheng, S.; Saito, T.; Novikov, V. N.; Sokolov, A. P. Hydrogen-bond Strength Changes Network Dynamics in Associating Telechelic PDMS. *Soft Matter* **2018**, *14*, 1235−1246.
(44) Floudas, G.; Fytas, G.; Pispas, S.; Hadjichristidis, N.; Pakula, T.; Khokhlov, A. R. Statics and Dynamics of .omega.-Functionalized Block Copolymers of Styrene and Isoprene. *Macromolecules* **1995**, *28*, 5109−5118.
(45) Floudas, G. Effects of Pressure on Systems with Intrinsic Orientational Order. *Prog. Polym. Sci.* **2004**, *29*, 1143−1171.
(46) Hadjichristidis, N.; Iatrou, H.; Pispas, S.; Pitsikalis, M. Anionic Polymerization: High Vacuum Techniques. *J. Polym. Sci., Part A: Polym. Chem.* **2000**, *38*, 3211−3234.
(47) Bhaumik, S.; Ntetsikas, K.; Hadjichristidis, N. Noncovalent Supramolecular Diblock Copolymers: Synthesis and Microphase Separation. *Macromolecules* **2020**, *53*, 6682−6689.
(48) Kremer, F.; Schönhals, A. *Broadband Dielectric Spectroscopy*; Springer: Berlin, 2002.
(49) Floudas, G. Dielectric Spectroscopy. In *Polymer Science: A Comprehensive Reference*; Matyjaszewski, K., Möller, M., Eds.; Elsevier BV: Amsterdam, 2012; Vol. 2.32, pp 825−845.
(50) Havriliak, S.; Negami, S. A Complex Plane Representation of Dielectric and Mechanical Relaxation Processes in Some Polymers. *Polymer* **1967**, *8*, 161−210.
(51) Milner, S. T.; McLeish, T. C. B. Parameter-free theory for stress relaxation in star polymer melts. *Macromolecules* **1997**, *30*, 2159−2166.
(52) Kardasis, P.; Oikonomopoulos, A.; Sakellariou, G.; Steinhart, M.; Floudas, G. Effect of Star Architecture on the Dynamics of 1,4-cis-Polyisoprene under Nanometer Confinement. *Macromolecules* **2021**, *54*, 11392−11403.
(53) Watanabe, H.; Matsumiya, Y.; Kwon, Y. Viscoelastic and Dielectric Relaxation of Reptating Type-A Chains Affected by Reversible Head-to-Head Association and Dissociation. *Macromolecules* **2018**, *51*, 6476−6496.
(54) Gambino, T.; Martínez de Ilarduya, A. M.; Alegría, A.; Barroso-Bujans, F. Dielectric Relaxations in Poly(glycidyl phenyl ether): Effects of Microstructure and Cyclic Topology. *Macromolecules* **2016**, *49*, 1060−1069.
(55) Ochs, J.; Veloso, A.; Martínez-Tong, D. E.; Alegria, A.; Barroso-Bujans, F. An Insight into the Anionic Ring-Opening Polymerization with Tetrabutylammonium Azide for the Generation of Pure Cyclic Poly(glycidyl phenyl ether). *Macromolecules* **2018**, *51*, 2447−2455.
(56) Paluch, M.; Patkowski, A.; Fischer, E. W. Temperature and Pressure Scaling of the α Relaxation Process in Fragile Glass Formers: A Dynamic Light Scattering Study. *Phys. Rev. Lett.* **2000**, *85*, 2140.
(57) Floudas, G.; Paluch, M.; Grzybowski, A.; Ngai, K. *Molecular Dynamics of Glass-Forming Systems: Effects of Pressure*; Springer Science & Business Media, 2010; Vol. *1*.
(58) Floudas, G.; Fytas, G.; Reisinger, T.; Wegner, G. Pressure-induced Dynamic Homogeneity in an Athermal Diblock Copolymer Melt. *J. Chem. Phys.* **1999**, *111*, 9129−9132.
(59) Andersson, S. P.; Andersson, O. Relaxation Studies of Poly(propylene glycol) Under High Pressure. *Macromolecules* **1998**, *31*, 2999.
(60) Alexandris, S.; Sakellariou, G.; Steinhart, M.; Floudas, G. Dynamics of Unentangled *cis*-1,4-Polyisoprene Confined to Nanoporous Alumina. *Macromolecules* **2014**, *47*, 3895−3900.
(61) Politidis, C.; Alexandris, S.; Sakellariou, G.; Steinhart, M.; Floudas, G. Dynamics of Entangled cis-1,4-Polyisoprene Confined to Nanoporous Alumina. *Macromolecules* **2019**, *52*, 4185−4195.
(62) Pipertzis, A.; Hossain, M. D.; Monteiro, M. J.; Floudas, G. Segmental Dynamics in Multicyclic Polystyrenes. *Macromolecules* **2018**, *51*, 1488−1497.
(63) Ngai, K. L.; Floudas, G.; Rizos, A. K.; Plazek, D. J. Amorphous Polymers. In *Encyclopedia of Polymer Properties*; John Wiley & Sons: New York, 2002.
(64) Rouse, P. E. A. A Theory of the Linear Viscoelastic Properties of Dilute Solutions of Coiling Polymers. *J. Chem. Phys.* **1953**, *21*, 1272−1280.
(65) Doi, M., Edwards, S. *The Theory of Polymer Dynamics*; Oxford University Press, 1986.
(66) Fetters, L. J.; Lohse, D. J.; Milner, S. T.; Graessley, W. W. Packing Length Influence in Linear Polymer Melts on the Entanglement, Critical, and Reptation Molecular Weights. *Macromolecules* **1999**, *32*, 6847−6851.
(67) Fetters, L. J.; Lohse, D. J.; Colby, R. H. *Physical Properties of Polymers Handbook*; Mark, J. E., Ed.; AIP Press: Woodbury, NY, 1996; p 335.
(68) Obukhov, S. P.; Rubinstein, M.; Duke, T. Dynamics of a Ring Polymer in a Gel. *Phys. Rev. Lett.* **1994**, *73*, 1263.
(69) Richter, D.; Goosßen, S.; Wischnewski, A. Celebrating Soft Matter's 10th Anniversary: Topology matters: structure and dynamics of ring polymers. *Soft Matter* **2015**, *11*, 8535−8549.
(70) Kapnistos, M.; Lang, M.; Vlassopoulos, D.; Pyckhout-Hintzen, W.; Richter, D.; Cho, D.; Chang, T.; Rubinstein, M. Unexpected Power-law Stress Relaxation of Entangled Ring Polymers. *Nat. Mater.* **2008**, *7*, 997−1002.
(71) Osterwinter, C.; Schubert, C.; Tonhauser, C.; Wilms, D.; Frey, H.; Friedrich, C. Rheological Consequences of Hydrogen Bonding: Linear Viscoelastic Response of Linear Polyglycerol and Its Permethylated Analogues as a General Model for Hydroxyl-Functional Polymers. *Macromolecules* **2015**, *48*, 119−130.
(72) Callies, X.; Véchambre, C.; Fonteneau, C.; Pensec, S.; Chenal, J. M.; Chazeau, L.; Bouteiller, L.; Ducouret, G.; Creton, C. Linear Rheology of Supramolecular Polymers Center-Functionalized with Strong Stickers. *Macromolecules* **2015**, *48*, 7320−7326.
(73) Kwon, Y.; Matsumiya, Y.; Watanabe, H. Viscoelastic and Orientational Relaxation of Linear and Ring Rouse Chains Undergoing Reversible End-Association and Dissociation. *Macromolecules* **2016**, *49*, 3593−3607.

https://doi.org/10.1021/acs.macromol.2c01527
Macromolecules 2022, 55, 10491−10501